

# An update to the Mathematica package PCR for simulation of planar channeling of electrons

Christopher Lynn

Department of Physics, Swarthmore College, Swarthmore, PA, 19081, USA

Tanaji Sen

Accelerator Physics Center, Fermi National Accelerator Laboratory, Batavia, IL, 60510, USA

August 22, 2013

## Abstract

The presented Mathematica package is an upgrade of the Mathematica package PCR presented by B. Azadegan [1]. The purpose of the package is to accurately and efficiently calculate the characterizing features of planar channeling radiation of relativistic electrons along major crystallographic planes of diamond, silicon, and germanium crystal. The package is based on the quantum theory of electron channeling as written by Azadegan in his dissertation which has been successfully applied to model planar channeling of electrons at energies between 10 and 100 MeV [2]. It will be shown that the PCR code is successful in calculating peak photon energies, but fails to generate accurate spectral linewidths and photon yields. The presented package adopts the successes of the PCR code: calculation of the continuum potentials for different planes of diamond, silicon, and germanium crystals; numerical solution of the one-dimensional Schrödinger equation; and calculation of the transition probabilities between channeling states. The package improves upon the spectral linewidths generated by the PCR code by including the effects of multiple scattering of electrons and Bloch-wave broadening as well as calculating a more accurate expression for the linewidth due to multiple scattering than is presented in Azadegan's dissertation. Finally, the package generates more accurate photon yields by including the dechanneling of electrons due to multiple scattering and the self-absorption of photons by the crystal, and convolving the Lorentzian line-shape of the PCR code with a Gaussian line-shape. The simulation of channeling radiation spectra is a useful tool in the comparison of theory with experimental data.

## 1 Introduction

Since its prediction and first exact description of its features by M.A. Kumakhov in 1976, many experiments have investigated the spectrum of channeling radiation (CR) of electrons in crystals. Of direct interest to this project are two experiments that are set to take place at Fermilab over the next year. The first of these, located at the A0 facility at Fermilab, will investigate the CR spectrum of low-energy electrons (3-5 MeV) in a diamond crystal of 10-micron thickness. The second, located at the Advanced Superconducting Test Accelerator (ASTA) facility at Fermilab, will investigate CR due to medium-energy electrons with very low emittance.

The understanding of experimental CR data will be facilitated by an accurate and efficient simulation code. The presented code builds upon the successes of the PCR package, written by Azadegan, while addressing its discrepancies with previous calculations done by Azadegan (2).

The product is a user-friendly Mathematica code that simulates planar CR of electrons in a single diamond crystal.

## 2 Background Theory

Planar electron channeling is the steering of electrons through crystallographic planes. When relativistic electrons are directed towards a randomly-oriented crystal, they are incoherently scattered off of individual atoms, producing polychromatic bremsstrahlung radiation. Channeling occurs when the electrons are directed nearly parallel to a crystallographic plane or axis. In the inertial frame of the electrons the planes appear continuous (instead of being composed of individual crystal atoms) and the electrons see a continuum interplanar potential in the direction perpendicular (transverse) to their motion.

In the classical interpretation of electron channeling, the electrons oscillate within the continuum potential. This approximation is valid for high electron energies (above 100 MeV) because the number of bound quantum states becomes large and the electrons can be thought of as moving continuously between them. At medium energies (between 10 MeV and 100 MeV), a quantum-mechanical approach must be taken.

### 2.1 Peak photon energies

In the inertial frame of the electrons, the continuum interplanar potential  $V(x)$  gives rise to a one-dimensional Schrödinger equation that reads [1]

$$\frac{-\hbar^2}{2\gamma m} \frac{d^2\psi(x)}{dx^2} + V(x)\psi(x) = E\psi(x) \quad (1)$$

where  $\hbar$  is the Planck constant,  $m$  is the rest mass of the electron, and  $x$  denotes the transverse direction perpendicular to crystal plane. Because the continuum potential is periodic (with the periodicity of the crystal planes), the solutions to Eq. 1 are Bloch waves [1]

$$\psi(x) = e^{ikx} \sum_n c_{k,n} e^{ingx} \quad (n = \dots, -1, 0, 1, \dots) \quad (2)$$

where  $g = \frac{2\pi}{d_p}$  is the reciprocal lattice vector of the plane in momentum space,  $d_p$  is the distance between adjacent planes, and  $k$  is the transverse crystal momentum.

The continuum potential can be expressed as a Fourier series [1]

$$V(x) = \sum_n v_n e^{ingx} \quad (n = \dots, -1, 0, 1, \dots) \quad (3)$$

with Fourier coefficients  $v_n$  calculated using the thermal-averaged Doyle-Turner approximation to electron scattering. Substituting Eqs. 2 and 3 into Eq. 1 reduces the problem to calculation of eigenvectors  $c_{k,n}$  and eigenvalues  $\epsilon_{k,n}$  which Mathematica handles very nicely.

In the frame of the electrons, the photon released in the transition from state  $i$  to state  $f$  at crystal momentum  $k$  will have energy  $\epsilon_{k,i} - \epsilon_{k,f}$ . In the rest frame of the lab, a photon emitted in the forward direction of the electrons will undergo a Doppler shift and have energy [1]

$$E_{k,0} = 2\gamma^2(\epsilon_{k,i} - \epsilon_{k,f}) \quad (4)$$

where  $\gamma$  is the relativistic gamma of the electrons. This is the peak photon energy for the  $i \rightarrow f$  transition.

### 2.2 Line broadening sources

The intrinsic CR line width is due to a combination of three main broadening effects.

### 2.2.1 Coherence length

The first of these broadening sources is the finite lifetime of the bound states in the interplanar potential. The lifetime is finite mainly due to thermal scattering or scattering off lightly bound electrons in crystal atoms. The line shape that results is a Lorentzian with a width given by [2]

$$\Gamma_{CL} = \frac{2\gamma^2 \hbar c}{l} \quad (5)$$

where  $\gamma$  is again the relativistic gamma of the electrons and  $l$  is the total coherence length given by [2]

$$\frac{1}{l} = \frac{1}{l_i} + \frac{1}{l_f} \quad (6)$$

where  $l_i$  and  $l_f$  are the coherence lengths of the initial and final states of the transition being considered.

Using the formalism of the complex potential,  $U(x) = V(x) + iW(x)$ , the coherence length of channeling state  $n$  is given by [1]

$$l_n = \frac{\hbar\beta c}{2\langle\psi_{k,n}|W|\psi_{k,n}\rangle} \quad (7)$$

where  $\beta = v/c$  and  $\langle\psi_{k,n}|W|\psi_{k,n}\rangle$  is the expectation value of the imaginary part of the complex potential for the state  $n$ . Thus, the expectation value of the imaginary potential, in part, characterizes the lifetime of that state.

### 2.2.2 Multiple scattering

The other factor that partially determines the lifetimes of channeling states is the multiple scattering of electrons off of crystal atoms. Multiple scattering of the electrons in the crystal increases the beam divergence and leads to CR line broadening and asymmetry. The photon energies have a Lorentzian distribution with respect to the scattering angle due Doppler shift that reads

$$E_\gamma(\theta) = \frac{E_0}{1 - \beta \cos(\theta)} \approx \frac{E_0}{1 + \gamma^2 \theta^2} \quad (8)$$

where  $\theta$  is the scattering angle and  $E_0$  is the peak photon energy of the transition.

The scattering angle of electrons has a Gaussian distribution with a standard deviation  $\theta_{ms,ch}$  called the rms channeling multiple scattering angle, given by [2]

$$f(\theta) = \frac{1}{\sqrt{2\pi}\theta_{ms,ch}} \exp\left(\frac{-\theta^2}{2\theta_{ms,ch}^2}\right) \quad (9)$$

The photon energy is averaged over this Gaussian distribution in scattering angle, giving

$$\langle E_\gamma \rangle = \frac{E_0}{\sqrt{2\pi}\theta_{ms,ch}} \int_{-\infty}^{\infty} \exp\left(\frac{-\theta^2}{2\theta_{ms,ch}^2}\right) \frac{1}{1 + \gamma^2 \theta^2} d\theta. \quad (10)$$

The line width due to multiple scattering is then given by

$$\Gamma_{MS} = \sqrt{\langle E_\gamma^2 \rangle - \langle E_\gamma \rangle^2} \quad (11)$$

It will later be shown that this expression is more accurate than the expression given by Azadegan in his dissertation and can thus be seen not only as an improvement to the PCR code but also to the theory as a whole.

### 2.2.3 Bloch-wave broadening

The eigenstates of the channeled electrons do not correspond to singular energy eigenvalues. Instead, each eigenstate has an energy band (or range) that depends on  $k$ , the crystal momentum. Within each band, the crystal momentum lies within the range  $-\pi/d_p \leq k \leq \pi/d_p$  and the maximum and minimum energies in a band occur at  $k_{max} = \pi/d_p$  and  $k_0 = 0$  (not necessarily respectively).

The energy bands allow for CR line broadening because the energies of the initial and final states for any given transition are not well-defined. The broadening that occurs is called Bloch-wave broadening and for small observation angles, it is given by the Doppler-shifted sum of the band widths of the initial and final states [2].

$$\Gamma_{BW} = 2\gamma^2(|\epsilon_{k_0,i} - \epsilon_{k_{max},i}| + |\epsilon_{k_0,f} - \epsilon_{k_{max},f}|) \quad (12)$$

### 2.2.4 Other line broadening sources

Another possible source of line broadening is the energy spread of the beam. The energy  $E_0$  of a CR peak scales with the energy of the beam  $E_e$  like [2]

$$E_\gamma \propto \gamma^a \quad (13)$$

where  $a$  is a constant that ranges between 1.5 and 2 depending on the transition being considered. The photon energy spread resulting from an initial beam energy spread is given by [2]

$$\frac{\Delta E_\gamma}{E_\gamma} = a \frac{\Delta E_e}{E_e} \quad (14)$$

If the energy spread of the beam is small then this effect is negligible.

One final line broadening source is the resolution of the photon detector being used in an experiment. In general, the width of the response function of the X-ray detector significantly contributes to the CR line width. This source of line broadening may be added to the Mathematica package at a later date.

### 2.2.5 Line shape and total line width

The line broadening due to coherence length and Bloch-wave broadening are Lorentzian in shape. The shape of the multiple scattering effect (and the detector resolution effect for a Gaussian response function) is Gaussian. Therefore, the total line width of the CR peak cannot be simply calculated as a linear sum nor as a quadratic sum. This being said, the total line width is often estimated by summing the partial line widths in quadrature, such as [2]

$$\Gamma^2 = \Gamma_{CL}^2 + \Gamma_{MS}^2 + \Gamma_{BW}^2 (+\Gamma_{DR}^2) \quad (15)$$

where  $\Gamma_{DR}$  is the partial line width due to the detector resolution.

The CR line shape that results from the convolution of Lorentzian and Gaussian profiles is called a Voigt profile. The total line shape is given by the probability function [2]

$$P(E_\gamma) = \pi^{-3/2} \int_0^\infty \frac{t^{-1/2}(\Gamma_T/2)(1 + 2\alpha^2 t)e^{-t}}{(E_\gamma(1 + 2\alpha^2 t) - E_0)^2 + 0.25(1 + 2\alpha^2 t)^2 \Gamma_T^2} dt \quad (16)$$

where  $E_\gamma$  is the peak photon energy at scattering angle  $\theta$ ,  $E_0$  is the maximum photon energy at  $\theta = 0$ ,  $\Gamma_T$  is the linear sum of the partial linewidths due to coherence length and Bloch-wave

broadening and  $\alpha = \gamma\theta_{ms,ch}$  is determined by the beam energy and the rms channeling multiple scattering angle.

### 2.3 Photon yield

The photon yield (intensity) of the  $i \rightarrow f$  transition is the number of photons per steradian per electron, given by [2]

$$\frac{dN(i \rightarrow f)}{d\Omega} = \int_{line} \frac{d^2N(i \rightarrow f)}{d\Omega dE_\gamma} dE_\gamma \quad (17)$$

where, according to Azadegan, the number of photons per steradian per electron and per photon energy is given by [2]

$$\begin{aligned} \frac{d^2N(i \rightarrow f)}{d\Omega dE_\gamma} &= \frac{\alpha_0 \lambda_c^2}{\pi \hbar c} E_0(i \rightarrow f) |\langle \psi_f | \frac{d}{dx} | \psi_i \rangle|^2 \int_0^L \exp(-\mu(E_\gamma)(L-z)) P_i(z) dz \\ &\times \pi^{-3/2} \int_0^\infty \frac{t^{-1/2} (\Gamma_T/2) (1 + 2\alpha^2 t) e^{-t}}{(E_\gamma(1 + 2\alpha^2 t) - E_0)^2 + 0.25(1 + 2\alpha^2 t)^2 \Gamma_T^2} dt \quad (18) \end{aligned}$$

where  $\alpha_0$  is the fine structure constant,  $\lambda_c$  is the Compton wave length,  $E_0(i \rightarrow f)$  is the peak photon energy of the transition,  $\langle \psi_f | \frac{d}{dx} | \psi_i \rangle$  is the dipole matrix element, the first integral describes the population dynamics of state  $i$  with  $\mu(E_\gamma)$  the absorption coefficient of X-rays of energy  $E_\gamma$ , and the second integral describes the line shape of the CR peak.

#### 2.3.1 Dipole matrix elements

The dipole matrix element determines the transition strength between the states. The Bloch-waves, normalized to one interval of planes is given by [2]

$$\psi_i(x) = \frac{1}{\sqrt{d_p}} e^{ikx} \sum_{n=-m}^m c_n^i e^{ingx} \quad (19)$$

where  $c_n^i$  are the eigenvectors of the system, calculated by Mathematica, and satisfying [2]

$$\sum_{n=-m}^m (c_n^i)^* c_n^i = 1 \quad (20)$$

Therefore, the dipole matrix element for the  $i \rightarrow f$  transition reads

$$\langle \psi_f | \frac{d}{dx} | \psi_i \rangle = \frac{i2\pi}{d_p} \sum_n (c_n^f)^* c_n^i (ng + k) \quad (21)$$

#### 2.3.2 Population dynamics

The occupation  $P_i(z)$  of channeling state  $i$  at crystal depth  $z$  depends on the initial population of the state as well as scattering processes that populate and depopulate the state. The initial population of state  $i$  at incidence angle  $\phi$  is given by the square of the overlap of the Bloch-wave with the electron plane wave, such as [2]

$$P_{i,0}(\phi) = |\langle \psi_i | \exp(ik_x x) \rangle|^2 = \frac{1}{d_p} \left| \int_{-\frac{d_p}{2}}^{\frac{d_p}{2}} \psi_i \exp(ik_x x) dx \right|^2 \quad (22)$$

where  $k_x = p_x \phi / \hbar$  is the transverse momentum of the electron.

For a more realistic simulation, the initial state populations can be averaged over the Gaussian distribution in incident angle. The distribution of incidence angle, centered at  $\phi_0$  is given by [2]

$$f(\phi) = \frac{1}{\sqrt{2\pi}\sigma_\phi} \exp\left(-\frac{(\phi - \phi_0)^2}{2\sigma_\phi^2}\right) \quad (23)$$

where  $\sigma_\phi$  is the beam divergence. Including the beam divergence in the calculation of the initial state populations is an important improvement that is made in the Mathematica package.

For a small interval of crystal depth  $\delta z$ , the occupation advance of state  $i$  can be approximated by [1]

$$P_i(z + \delta z) \cong P_i(z) + \delta z \frac{dP_i(z)}{dz} \quad (24)$$

where  $\frac{dP_i(z)}{dz}$  is determined by the transition rate per unit length between states  $i$  and  $j$ ,  $T_{j,i}$ , such as [2]

$$\frac{dP_i(z)}{dz} = \sum_j T_{j,i}(P_j(z) - P_i(z)) \quad (25)$$

where  $T_{j,i}P_j(z)$  defines the feeding of state  $i$ , and  $T_{j,i}P_i(z)$  defines the depopulation of state  $i$ . The transition rates are defined by the overlap of the states  $i$  and  $j$  with the imaginary potential, such as [1]

$$T_{j,i} = T_{i,j} = \frac{2}{\hbar v} |\langle \psi_j | W | \psi_i \rangle| \quad (26)$$

### 2.3.3 Photon self-absorption

The final part of Eq. 18 left to be explained is the exponential term in the first integral,  $\exp(-\mu(E_\gamma)(L - z))$ , which describes the self-absorption of CR photons by the crystal. The absorption coefficient is defined by

$$\mu(E_\gamma) = \frac{1}{l_{abs}(E_\gamma)} \quad (27)$$

where  $l_{abs}(E_\gamma)$  is the absorption length of photons with energy  $E_\gamma$ . The absorption length also depends on the channeled substance. In diamond crystal, values of the absorption coefficient are well-defined and are listed in a database provided by the National Institute of Standards and Technology [4].

### 2.3.4 Dechanneling of electrons due to multiple scattering

One important factor that is not included in Eq. 18 and does not show up in the PCR code is the dechanneling of electrons due to multiple scattering in the crystal. Azadegan briefly addresses the topic of dechanneling in his dissertation, stating that the exponential term is only valid for thin crystals (less than 10 microns) while a fit of experimental photon yield data vs. crystal depth  $z$  reveals that the state populations more closely follow a  $z^{-1/2}$  dependence for all crystal thicknesses [2]. Azadegan goes on to state that this dependence can be shown but the authors have yet to find proper theoretical justification. In any case, the dechanneling of electrons is a very important factor in determining the photon yield of a CR peak and must be included in any accurate simulation.

## 3 Comparing PCR with theory and experiment

Before the PCR code could be improved, its discrepancies with Azadegan's theoretical calculations and experimental data had to be diagnosed and understood. The first step in this process was to compare calculations by the code of the three main spectral characteristics (photon energy, line width, and photon yield) with the calculations and experimental data in Azadegan's dissertation.

In his dissertation, Azadegan calculates and cites experimental measurements for beam energies and crystal thicknesses of 14.6 MeV: (42.5, 168, 500) microns, 17 MeV: (42.5, 102, 168, 500) microns, 30 MeV: (42.5, 102, 168, 500) microns, and 34 MeV: 42.5 microns for the  $1 \rightarrow 0$  transition in the (110) plane of a single diamond crystal. The PCR code was used to calculate the photon energies, linewidths, and yields of the same transition for beam energies of 5.2, 9, 14.6, 17, 21, 25, 30, and 34 MeV and crystal thicknesses of 42.5 and 168 microns each (except for 34 MeV for which only 42.5 micron-thick diamond was considered).

### 3.1 Peak photon energy

Figure 1: *Peak photon energy comparison of PCR code with Azadegan's calculations and measurement for the  $1 \rightarrow 0$  transition in the (110) plane of diamond, 42.5 microns thick. The PCR calculations closely match both Azadegan's calculations and experimental data.*

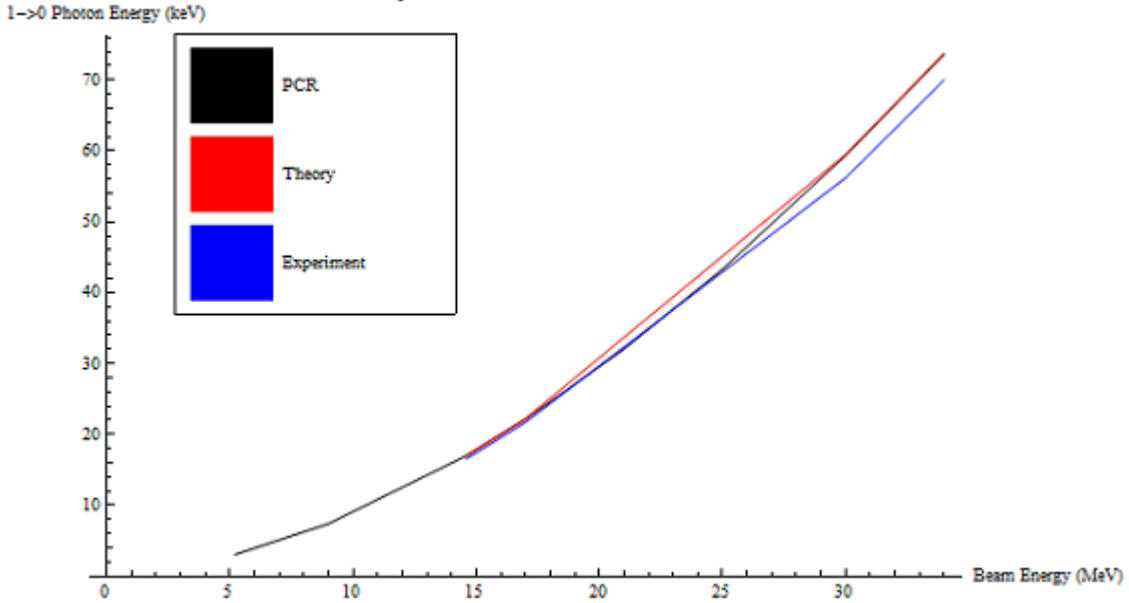


Table 1: *PCR, calculated, and measured peak CR photon energies of the  $1 \rightarrow 0$  transition in the (110) plane of diamond.*

$L$ ( $\mu\text{m}$ )	$E_{PCR(k_0)}$ (keV)	$E_{calc}$ (keV)	$E_{exp}$ (keV)
14.6 MeV			
42.5	17.01	17.06	16.58
168	17.01	17.06	16.99
17 MeV			
42.5	22.17	22.23	21.72
168	22.17	22.23	21.42
30 MeV			
42.5	59.34	59.49	56.19
168	59.34	59.49	56.22
34 MeV			
42.5	73.57	73.78	70.02

The calculated peak photon energies from the PCR code (for crystal momentum  $k_0 = 0$ ) are

compared with the calculations and experimental data from Azadegan’s dissertation. The peak photon energies do not change significantly with crystal momentum so  $k_0$  was chosen by default. Fig. 1 shows the peak photon energy (keV) vs. beam energy (MeV) for the (110) plane of 42.5-micron-thick diamond and Tab. 1 displays all comparison data for the peak photon energy. It is important to note that in Fig. 1 and Tab. 1 as well as the following comparison plots and tables, the label "Theory" or subscript "calc" represents the calculations done by Azadegan based on the theory written in his dissertation and "Experiment" or "exp" represents the experimental measurements cited in his dissertation [2].

It can be seen from Tab. 1 that the peak photon energies are independent of crystal thickness. The PCR data differs from Azadegan’s calculations by a maximum of 5 percent. This is satisfactory and there was no need to make alterations to the portions of the PCR code involved in calculating peak photon energies.

### 3.2 Total line width

The PCR code prints out the total CR line width for each transition at the completion of a simulation. In Fig. 2 and Fig. 3, the PCR-calculated total line widths (keV) for  $k_0$  are compared with Azadegan’s calculations and measurements for 42.5- and 168-micron-thick diamond, respectively, versus beam energy (MeV). Tab. 2 displays the comparison data.

Looking at Fig. 2 and Fig. 3, the first striking feature is that the PCR-calculated linewidths are significantly lower than the theoretically-calculated linewidths. Tab. 2 presents another disturbing feature - the PCR-calculated linewidths do not change with crystal thickness, but both the theoretical calculations and measurements increase. Further investigation into the calculation of linewidths in the PCR code were necessary to determine the source of the discrepancy.

Figure 2: *Total line width comparison of PCR code with Azadegan’s calculations and measurement for the  $1 \rightarrow 0$  transition in the (110) plane of diamond, 42.5 microns thick. The PCR calculations are significantly lower than both Azadegan’s calculations and experimental data.*

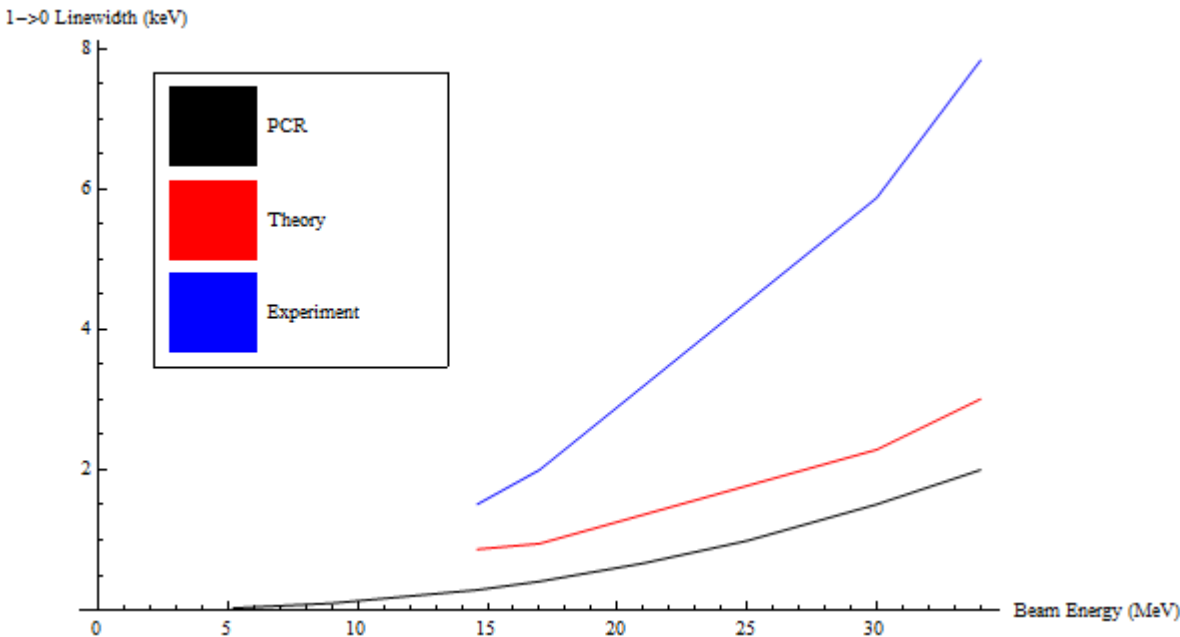


Figure 3: Total line width comparison of PCR code with Azadegan’s calculations and measurement for the  $1 \rightarrow 0$  transition in the  $(110)$  plane of diamond, 168 microns thick. The difference between PCR calculations and both Azadegan’s calculations and experimental data has grown with increasing crystal thickness.

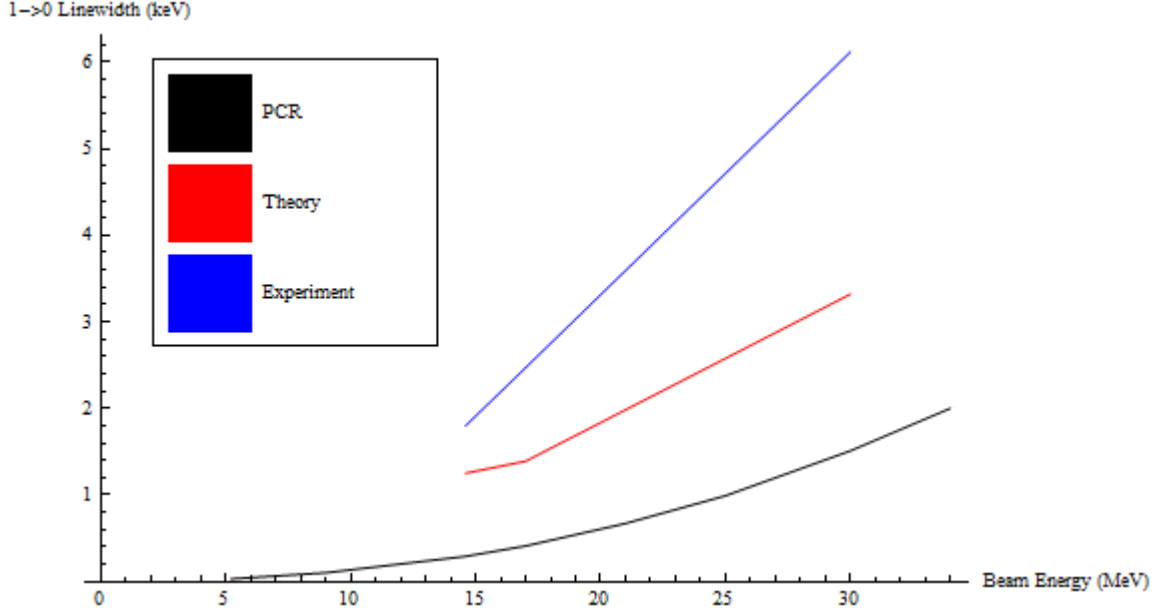


Table 2: PCR, calculated, and measured CR line widths of the  $1 \rightarrow 0$  transition in the  $(110)$  plane of diamond.

$L$ ( $\mu\text{m}$ )	$\Gamma_{PCR(k_0)}$ (keV)	$\Gamma_{calc}$ (keV)	$\Gamma_{exp}$ (keV)
14.6 MeV			
42.5	0.29	0.87	1.51
168	0.29	1.25	1.80
17 MeV			
42.5	0.41	0.95	2.00
168	0.41	1.39	2.47
30 MeV			
42.5	1.51	2.29	5.88
168	1.51	3.32	6.12
34 MeV			
42.5	2.00	3.01	7.84

### 3.3 Photon yield

The PCR code also prints out the photon yield per steradian and per electron for each transition at the completion of a simulation. At zero incidence angle, and zero crystal momentum, the  $n = 1$  state is never populated and thus there are no photons emitted for the  $1 \rightarrow 0$  peak. It is for this reason that we consider the PCR-calculated photon yields at  $k_{min} = \pi/5d_p$  instead of  $k_0$ . Fig. 4 and Fig. 5 compare the PCR-calculated photon yields with Azadegan’s calculated and measured photon yields for 42.5- and 168-micron-thick diamond versus beam energy, respectively. Tab. 3

Figure 4: Photon yield comparison of PCR code with Azadegan's calculations and measurement for the  $1 \rightarrow 0$  transition in the  $(110)$  plane of 42.5-micron-thick diamond. The PCR calculations are significantly greater than both Azadegan's calculations and experimental data and the discrepancy increases with beam energy.

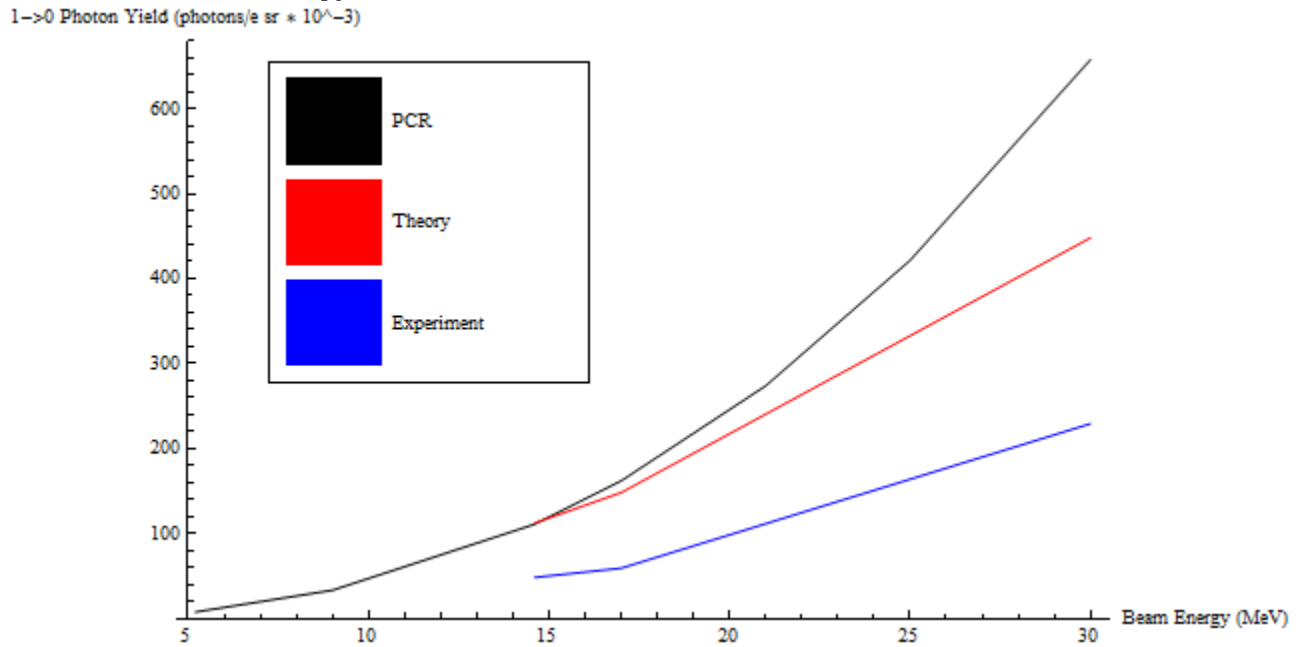


Figure 5: Photon yield comparison of PCR code with Azadegan's calculations and measurement for the  $1 \rightarrow 0$  transition in the  $(110)$  plane of 168-micron-thick diamond. The difference between PCR calculations and both Azadegan's calculations and experimental data has grown with increasing crystal thickness.

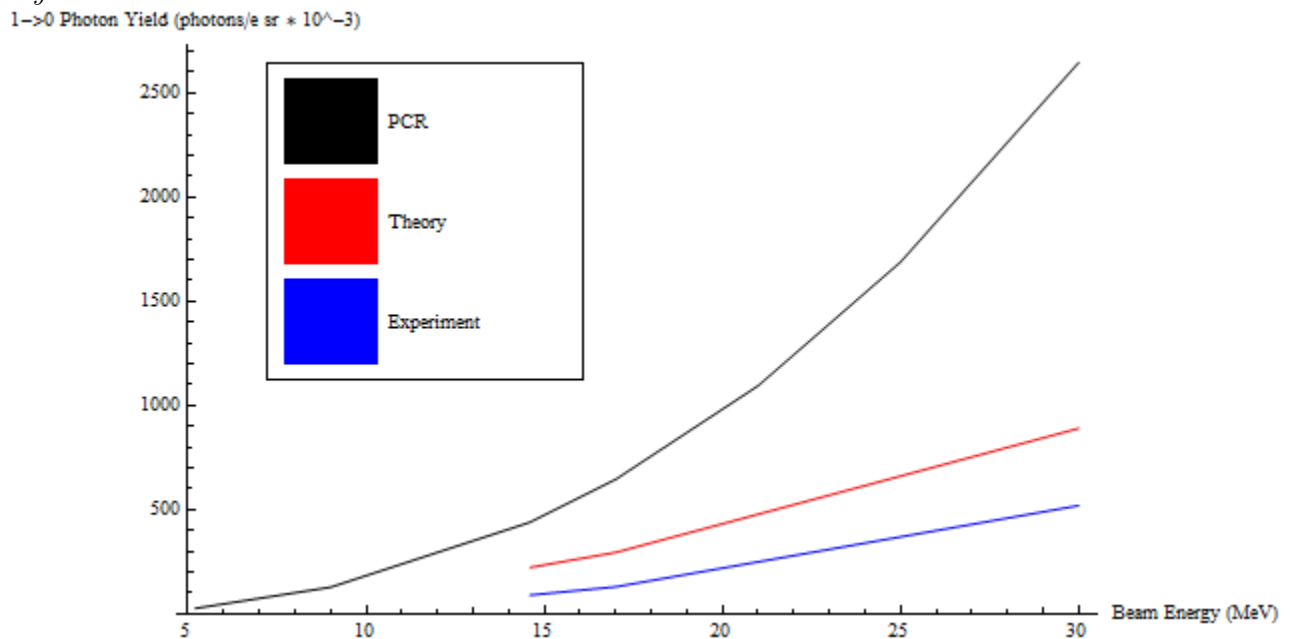


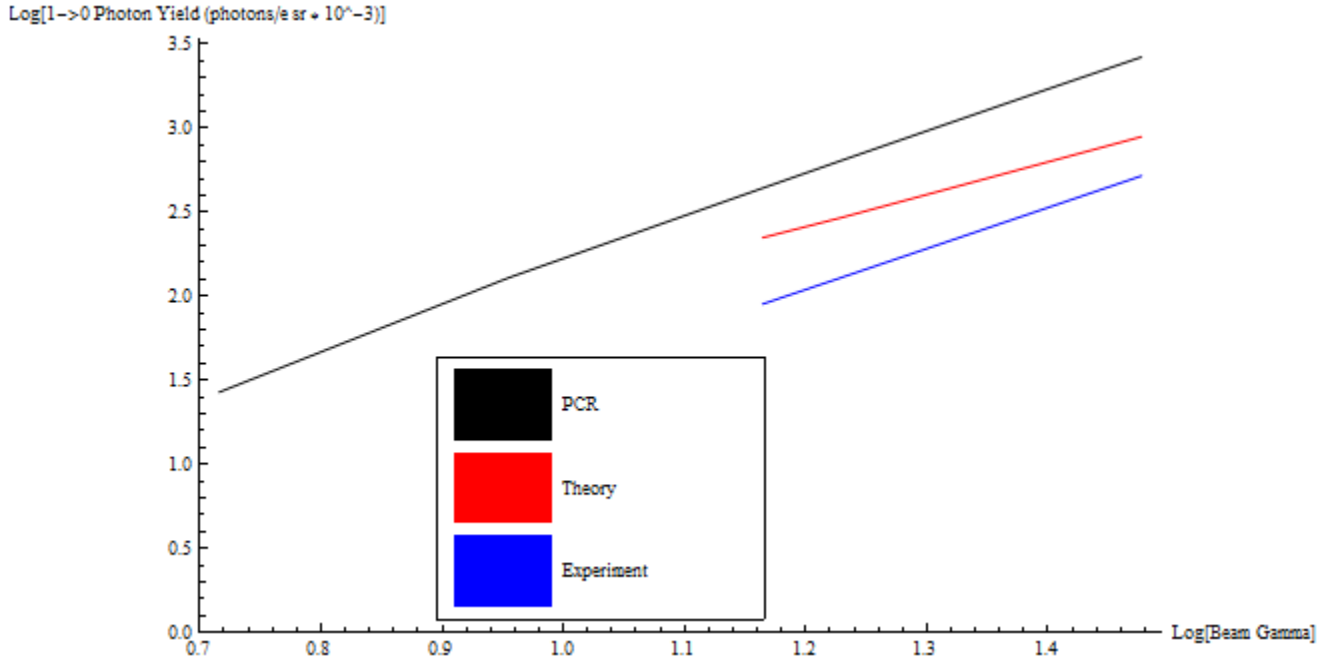
Table 3: PCR-calculated, theoretically-calculated, and measured CR photon yields of the  $1 \rightarrow 0$  transition in the (110) plane of diamond.

$L$ ( $\mu\text{m}$ )	$Y_{PCR(k_{min})}$ (photons/e sr $\cdot 10^{-3}$ )	$Y_{calc}$ (photons/e sr $\cdot 10^{-3}$ )	$Y_{exp}$ (photons/e sr $\cdot 10^{-3}$ )
14.6 MeV			
42.5	111	112	48
168	440	223	90
17 MeV			
42.5	162	148	59
168	645	295	130
30 MeV			
42.5	658	448	229
168	2645	890	520

presents the comparison data.

The PCR-calculated photon yields clearly overestimate the theoretical data and the discrepancy with Azadegan's data increases with both beam energy and crystal thickness. Fig. 6 shows a log-log fit of the photon yield data versus the beam gamma for 42.5-micron-thick diamond. Fitting Fig. 6, as well as data for 168-micron crystal thickness, reveals that the PCR photon yields increase approximately like  $\gamma^{2.5}$ , while the theoretical photon yields increase like  $\gamma^{1.93}$  and the measured yields increase approximately like  $\gamma^{2.3}$ .

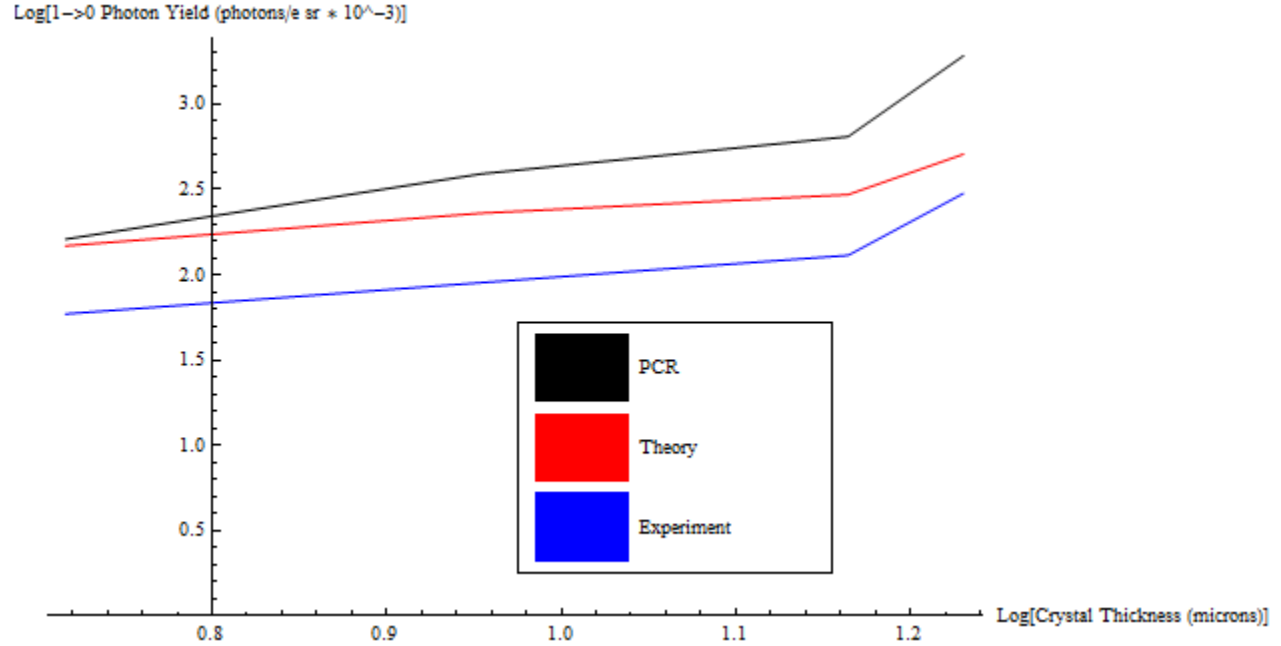
Figure 6: Log-log photon yield comparison of PCR code with Azadegan's calculations and measurement vs. beam gamma for the  $1 \rightarrow 0$  transition in the (110) plane of 42.5-micron-thick diamond. The slope for PCR is greater than Azadegan's theory but about the same as his measurements.



A similar analysis was done on the photon yield data versus crystal thickness. Fig. 7 is a log-log fit of the photon yields versus crystal thickness for a 17 MeV electron beam. The PCR photon yields are very nearly proportional to  $L$  while the theoretically-calculated yields are proportional to

$\sqrt{L}$  and the measured yields increase approximately like  $L^{.63}$ . The discrepancy between the PCR-calculated photon yields and the theoretically-calculated yields cited in Azadegan’s dissertation were troubling, especially with respect to the crystal thickness. Further investigation was necessary to determine the source of the discrepancy.

Figure 7: *Log-log photon yield comparison of PCR code with Azadegan’s calculations and measurement vs. crystal thickness for 17 MeV electrons undergoing the 1→0 transition in the (110) plane of diamond. The slope for PCR is nearly twice that of Azadegan’s theory and measurements.*



## 4 Improving PCR

Before improvements to line width and photon yield calculations of the code could be made, the sources of the discrepancies had to be understood. This required line-by-line comparison of the PCR code with the theoretical framework presented in Azadegan’s dissertation. Only twice, in the case of the partial linewidth due to multiple scattering and the dechanneling of electrons due to occupation length, was the theory actually improved. In all other cases, Azadegan simply did not include portions of the theory in the PCR code.

### 4.1 Fixing the line widths

In our comparison of PCR and theoretical calculations, it was shown that the PCR code significantly underestimates the line widths of CR spectral peaks. Upon analysis of the code, it was found that the PCR package only considers line broadening due to coherence length. In order to improve the code, calculation of partial line widths due to multiple scattering and Bloch-wave broadening were included. These three partial line-widths were then added in quadrature to give the total line width.

Including the Bloch-wave broadening was straightforward by use of the theory presented in Sec. 2.2.3. Including the line width due to multiple scattering was not quite as simple.

#### 4.1.1 Improving the line width due to multiple scattering

In Azadegan's dissertation he states that the Doppler broadening of planar CR due to multiple scattering can be evaluated by [2]

$$\Gamma_{Dopp} = \gamma^2 \theta_{ms,ch}^2 E_0 \quad (28)$$

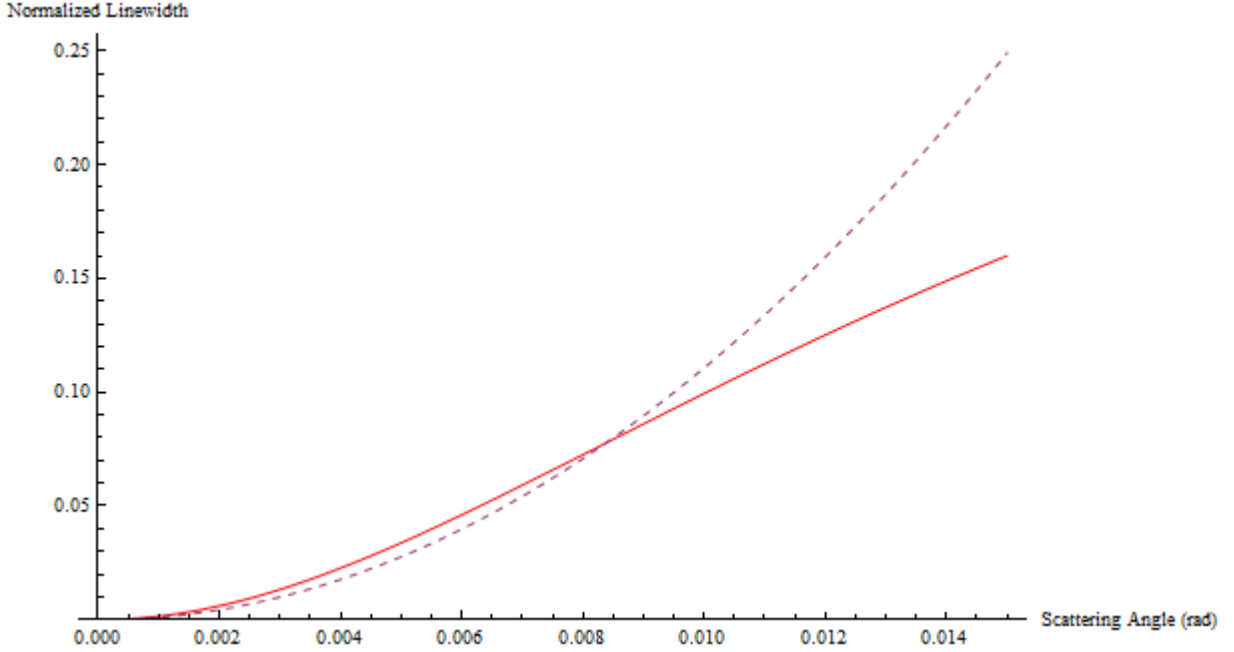
This is merely an approximation to the formulation

$$\Gamma_{MS} = \sqrt{\langle E_\gamma^2 \rangle - \langle E_\gamma \rangle^2} \quad (29)$$

presented in Sec. 2.2.2.

Interestingly,  $\Gamma_{MS}$  is greater than  $\Gamma_{Dopp}$  for approximately  $\theta_{ms,ch} < 10 \text{ mrad}$ , depending on the beam energy. This can be seen in Fig. 8.

Figure 8:  $\Gamma_{MS}$  (red) and  $\Gamma_{Dopp}$  (dashed) normalized by peak photon energy vs.  $\theta_{ms,ch}$  for the  $1 \rightarrow 0$  transition of 17 MeV electrons channeled in the (110) plane of diamond.  $\Gamma_{MS} > \Gamma_{Dopp}$  for approximately  $\theta_{ms,ch} < 10 \text{ mrad}$ .



In general, the rms multiple scattering angles are less than the angle at the point of crossing of  $\Gamma_{MS}$  and  $\Gamma_{Dopp}$  (about  $10 \text{ mrad}$ ). Thus, the partial line width due to multiple scattering is actually greater than Azadegan's approximation by up to 10 percent. This difference is large enough to be considered significant and decreases the difference between theory and experiment.

#### 4.1.2 An expression for the rms channeling multiple scattering angle

In order to apply the improved  $\Gamma_{MS}$  in the code, an expression for  $\theta_{ms,ch}$  is necessary. The rms multiple scattering angle of electrons in amorphous media is given by [2]

$$\theta_{ms} = \left( \frac{14 \text{ MeV}}{E_e} \right) \sqrt{\frac{z}{L_0}} \left( 1 + 0.038 \ln \frac{z}{L_0} \right) \quad (30)$$

where  $E_e$  is the beam energy,  $L_0$  is the radiation length (the path length after which the electron energy is diminished by a factor of  $\frac{1}{e}$  due to radiation losses), and  $z$  is the thickness of the layer. For a randomly-oriented diamond crystal, the radiation length is 12.23 cm. Unfortunately, the radiation lengths of diamond oriented along major crystallographic planes are not well-known. However, Azadegan obtains  $\theta_{ms,ch}$  by fitting CR lines measured for the  $1 \rightarrow 0$  transition of electrons channeled in the (110) plane of diamond. The values are listed in Tab. 4 [2].

Table 4: Mean channeling multiple scattering angles obtained by fits of CR lines measured for the  $1 \rightarrow 0$  transition in the (110) plane of diamond and ratios of the mean multiple scattering angles for channeling to the mean multiple scattering angles for a randomly oriented diamond crystal.

$E_e$ (MeV)	$\theta_{ms,ch}$ (mrad)	$\theta_{ms,ch}/\theta_{ms}$
42.5 $\mu\text{m}$		
14.6	6.03	0.55
17	5.32	0.56
30	2.87	0.54
34	2.60	0.56
102 $\mu\text{m}$		
17	6.33	0.41
30	3.69	0.42
168 $\mu\text{m}$		
14.6	8.62	0.36
17	6.91	0.33
30	3.84	0.33
500 $\mu\text{m}$		
14.6	9.73	0.22
17	8.46	0.22

The next step was to fit the  $\theta_{ms,ch}$  data from Tab. 4 vs. beam energy and crystal thickness. In his dissertation, Azadegan concludes that the dependence  $\theta_{ms,ch} \propto 1/E_e$  holds as given by Eq. 30. A log-log fit of the data verified this dependence. Fitting of a log-log plot of the  $\theta_{ms,ch}$  data against crystal thickness gives a dependence of approximately  $\theta_{ms,ch} \propto L^2$ . Finally, incorporating these proportionalities and fitting the data one more time to find the scale factor gives an approximate expression

$$\theta_{ms,ch} \approx c \frac{L^{0.2}}{E_e} \quad (31)$$

where  $c = .083$ . Fig. 9 and Fig. 10 show the fitted expression versus beam energy and crystal thickness, respectively, in comparison with  $\theta_{ms,ch}$  data from Tab. 4.

Eq. 31 provides an accurate expression for the mean multiple scattering angle for the (110) plane of diamond. In order to approximate  $\theta_{ms,ch}$  for the (100) and (111) planes of diamond, and possibly for germanium and silicon, fitting the ratio  $\frac{\theta_{ms,ch}}{\theta_{ms}}$  is more helpful. Calculating  $\theta_{ms}$  for a randomly-oriented crystal is simple using Eq. 30 and multiplication with the ratio yields an approximate  $\theta_{ms,ch}$  for the crystal. The accuracy of this approach must be verified, but it makes the calculation of  $\theta_{ms,ch}$  more general. For this reason, the fitting of  $\frac{\theta_{ms,ch}}{\theta_{ms}}$  with crystal thickness is one of the next steps in the project (it has already been shown that  $\frac{\theta_{ms,ch}}{\theta_{ms}}$  is constant with beam energy since  $\theta_{ms,ch} \propto \theta_{ms} \propto 1/E_e$ ).

Figure 9:  $\theta_{ms,ch}$  obtained by fitting Tab. 4 and data from Tab. 4 vs. beam energy for electrons channeled in the (110) plane of 42.5-micron-thick diamond.

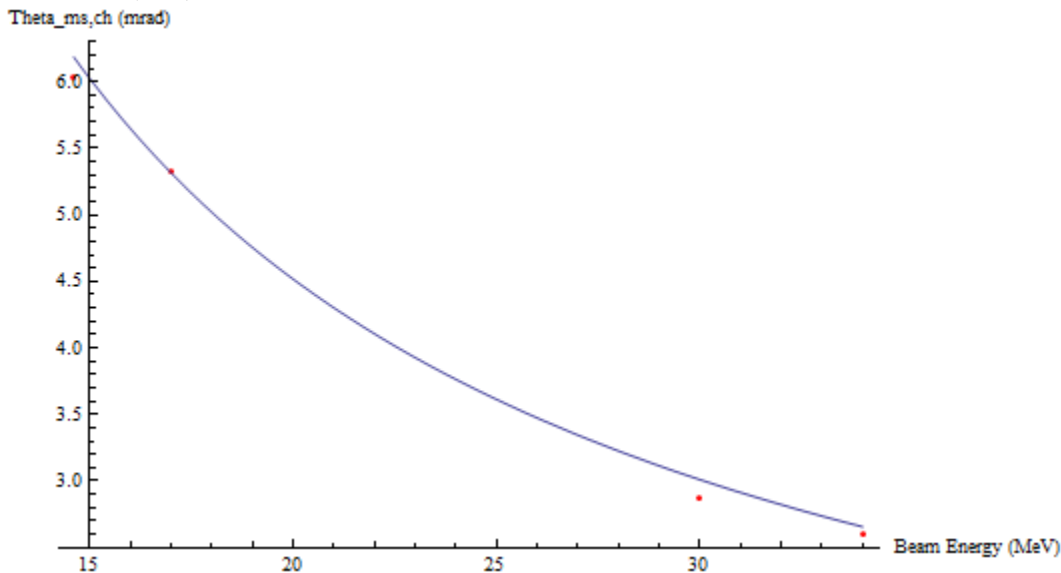
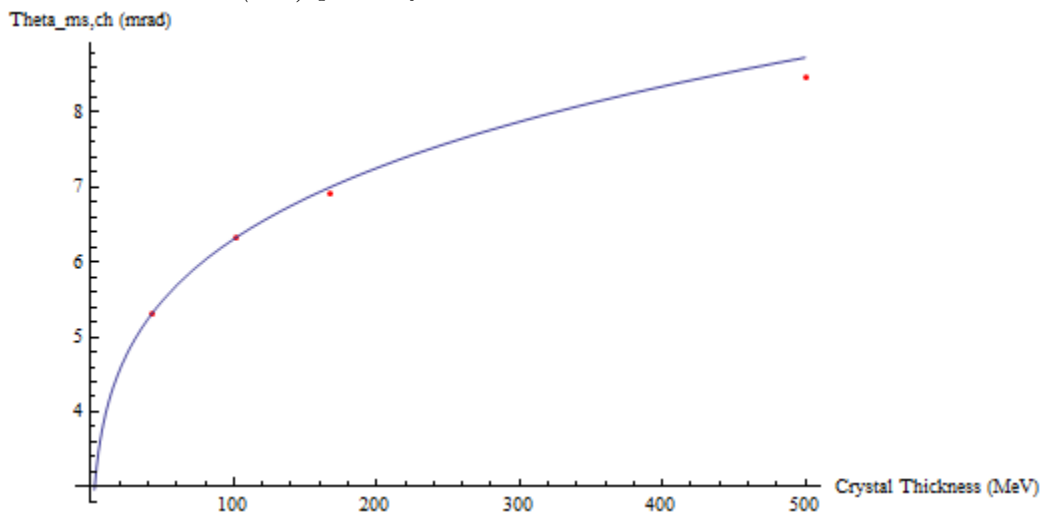


Figure 10:  $\theta_{ms,ch}$  obtained by fitting Tab. 4 and data from Tab. 4 vs. crystal thickness for 17 MeV electrons channeled in the (110) plane of diamond.



### 4.1.3 Total line width

Combining the partial line widths due to Bloch-wave broadening, multiple scattering, and coherence length, in quadrature like Eq. 15, gives the total line width. The partial line width due to Bloch-wave broadening is calculated using Eq. 12. The line width due to multiple scattering is calculated using Eq. 29, an improvement upon Azadegan's calculation, using Eq. 28. The line width due to coherence length is calculated by the PCR code using Eqs. 5-7. Figs. 11 and 12 compare the updated total line widths with Azadegan's calculations and measurements versus beam energy for the CR peak corresponding to the  $1 \rightarrow 0$  transition in the (110) plane of 42.5- and 168-micron-thick

Figure 11: Line width comparison of updated total line width with Azadegan's calculations and measurement for the  $1 \rightarrow 0$  transition in the  $(110)$  plane of 42.5-micron-thick diamond. The updated line widths, including Bloch-wave and multiple scattering effects, are close to Azadegan's calculations.

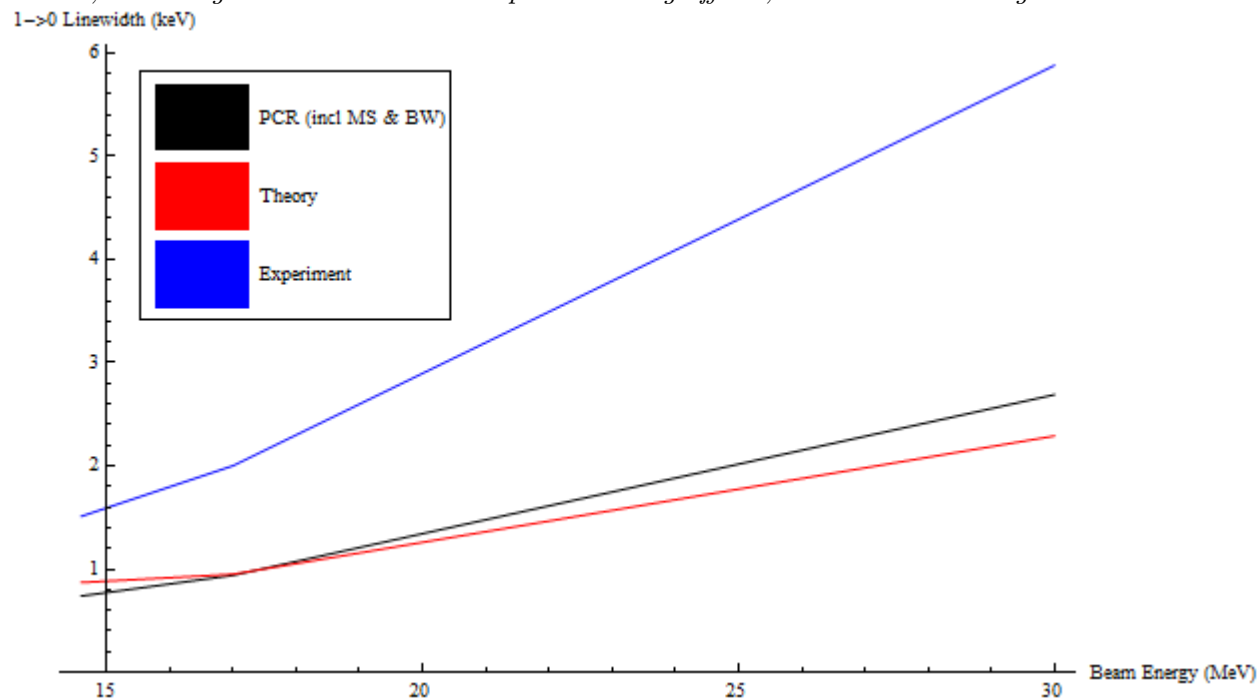


Figure 12: Line width comparison of updated total line width with Azadegan's calculations and measurement for the  $1 \rightarrow 0$  transition in the  $(110)$  plane of 168-micron-thick diamond. The updated line widths, including Bloch-wave and multiple scattering effects, are close to Azadegan's calculations.

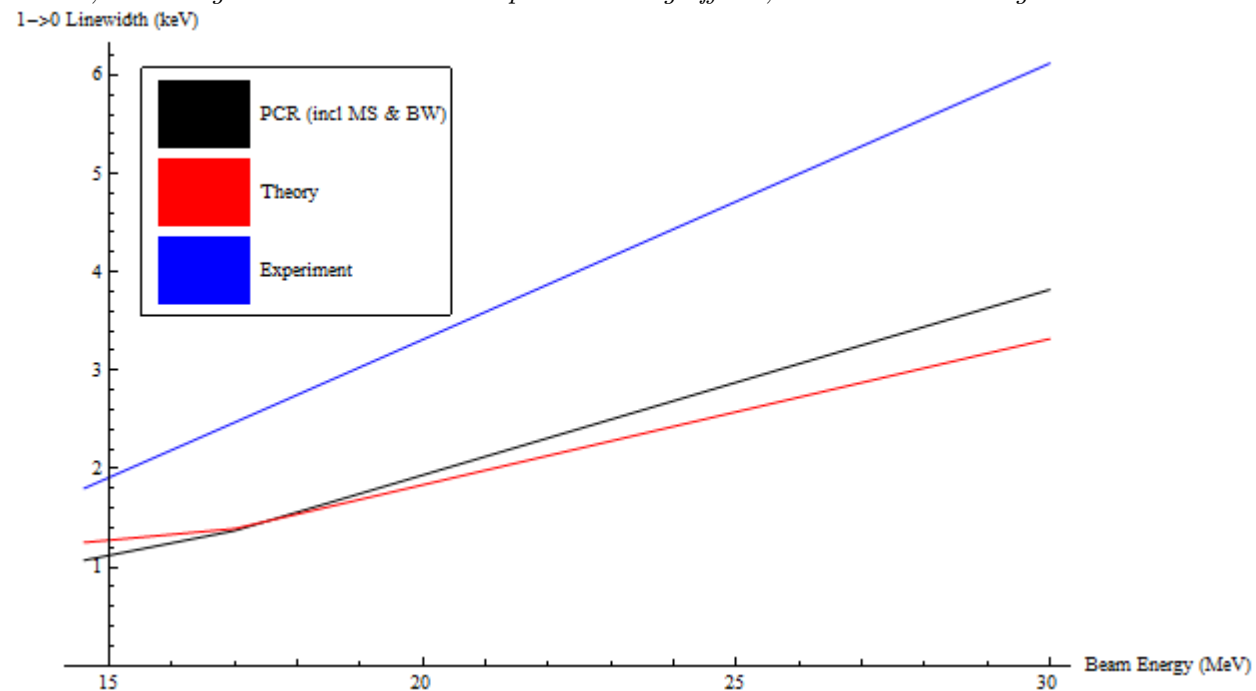


Table 5: Updated total line width including Bloch-wave and multiple scattering effects, theoretically-calculated, and measured CR line widths of the  $1 \rightarrow 0$  transition in the (110) plane of diamond.

$L$ ( $\mu\text{m}$ )	$\Gamma_{PCR(incl\ BW\&MS)}$ (keV)	$\Gamma_{calc}$ (keV)	$\Gamma_{exp}$ (keV)
14.6 MeV			
42.5	0.74	0.87	1.51
168	1.07	1.25	1.8
17 MeV			
42.5	0.94	0.95	2.00
168	1.37	1.39	2.47
30 MeV			
42.5	2.69	2.29	5.88
168	3.82	3.32	6.12

diamond, respectively, and Tab. 5 displays the data.

The updated total line widths, including Bloch-wave and multiple scattering effects, are very close to the calculations cited in Azadegan's dissertation. The existing difference with Azadegan's calculations is due to the improved expression for the multiple scattering linewidth and omission of the line-broadening effect of the detector resolution (which Azadegan includes). It is expected that the total line width will become closer to Azadegan's measurements once the partial line widths of detector resolution and beam energy spread are included.

## 4.2 Fixing the photon yields

Finding the sources of error in the photon yield calculations was more difficult than finding those of the line width. Calculation of the photon yield of a CR peak, defined by Eqs. 17 and 18, incorporates all of the CR theory discussed and is dependent upon almost every previous portion of the PCR code.

By comparison of the PCR code with theory, it was determined that each part of the code correctly fulfilled its intended purpose, leading to the conclusion that, again, Azadegan simply did not include parts of the theory in his code. Using proper notation, the equivalent of Eq. 18 in the code reads [3]

$$\frac{d^2 N(i \rightarrow f)}{d\Omega dE_\gamma} = \frac{\alpha_0 \lambda_c^2}{\pi \hbar c} E_0(i \rightarrow f) |\langle \psi_f | \frac{d}{dx} | \psi_i \rangle|^2 \int_0^L P_i(z) dz (\pi^{-1} \frac{\Gamma_{CL}/2}{(E_\gamma - E_0)^2 + 0.25 \Gamma_{CL}^2}) \quad (32)$$

The two glaring differences between Eq. 32 and Eq. 18 are the omission of the exponential factor in the first integral, which defines the self-absorption of photons, and the replacement of the entire second integral describing the convolved Lorentzian-Gaussian line shape, with a Lorentzian shape of width  $\Gamma_{CL}$ .

### 4.2.1 Including photon self-absorption

The exponential term  $\exp(-\mu(E_\gamma)(L - z))$  seems straightforward to implement in the code. In diamond crystal, values of the absorption coefficient range from  $.782 \mu\text{m}^{-1}$  for photons of 1 keV to  $2.24\text{E-}5 \mu\text{m}^{-1}$  for 1 MeV photons [4]. Using built-in Mathematica commands, an interpolation function was created for  $\mu(E_\gamma)$ .

Upon implementation, it was found that for thin crystals (less than about  $50 \mu\text{m}$ ), the second integral in Eq. 18 did not converge quickly enough and the program would crash. For thick crystals the program ran smoothly, but the net effect was minimal. The photon yield calculations were

decreased by about 2 to 3 percent, a far cry from the approximately 80 percent change necessary for the code to be consistent with Azadegan’s photon yield calculations.

A final decision on whether or not to implement the self-absorption factor is pending. One possibility would be to use a linear approximation to the exponential term, but this introduces an error in the effect of about 50 percent.

#### 4.2.2 Changing the line shape

In the PCR code, Azadegan uses a purely Lorentzian line shape because he only incorporates line broadening due to coherence length. A more accurate expression for the line width, including effects from Bloch-wave broadening (also Lorentzian in shape) and multiple scattering (Gaussian shape), necessitates the use of a convolution of Lorentzian and Gaussian line shapes.

The second integral in Eq. 18 is the convolution of Lorentzian and Gaussian line shapes. It is obtained by averaging a Lorentzian distribution in photon energy of width  $\Gamma_T$  over a Gaussian distribution in scattering angle of width  $\theta_{ms,ch}$ . The values of  $\theta_{ms,ch}$  in  $\alpha$  in Eq. 18 are obtained by use of the fit expression presented in Sec. 4.1.2.

The implementation of the new line shape was successful, but only decreased the photon yield calculations by about 5 percent. Again, this is far from the approximately 80 percent drop needed to explain the discrepancy with theory. This was troubling because even after the yield calculations of the PCR code were altered to match Eqs. 17 and 18, they still did not match Azadegan’s calculations.

#### 4.2.3 Dechanneling of electrons due to multiple scattering

After the two obvious differences between Eqs. 18 and 32 were addressed, there was still a large discrepancy between photon yield calculations by PCR and those cited in Azadegan’s dissertation. A comparison showed no difference between the code and the theory cited by Azadegan. To be thorough, a paper by Chouffani, cited extensively in Azadegan’s dissertation, was checked against the theory in Azadegan’s dissertation [5]. It was found that Azadegan did not include the effect of dechanneling of electrons in the theory he presents nor in his code, while Chouffani provides a theoretical expression.

In the code, the population of the channeling state  $i$  at a given crystal depth,  $P_i(z)$ , is calculated using Eqs. 24-26. Eq. 25 accounts only for the depopulation of state  $i$  by nonradiative transition to state  $j$  and population of state  $i$  from particles in state  $j$ . In this framework, there is no net loss of electrons to dechanneling. Chouffani includes the dechanneling of electrons due to multiple scattering off the crystal atoms by adding a second term in Eq. 25, such as [5]

$$\frac{dP_i(z)}{dz} = \sum_n T_{n,i}(P_n(z) - P_i(z)) - \sum_m T_{m,i}P_i(z) \quad (33)$$

where the first term sums over the bound states and the second term sums over the unbound states.

Substituting Eq. 33 for Eq. 25 in the code was simple. Figs. 13 and 14 are comparisons of the new photon yields, including dechanneling effects, with the calculations and measurements cited in Azadegan’s dissertation for crystal thicknesses of 42.5 and 168 microns respectively. Tab. 6 shows the data in Figs. 13 and 14.

Including the dechanneling effect, the photon yield calculations of the code are in close agreement with Azadegan’s calculations and measurement, and almost exactly match Azadegan’s calculations at beam energies around 20 - 22 MeV. Yet, it can be seen that the photon yield calculations of the code with the dechanneling effect still increase too sharply with increasing beam energy. A full analysis of the shape of the new photon yield calculations versus beam energy and crystal thickness must be done.

Figure 13: Photon yield comparison of PCR code, including dechanneling effects, with Azadegan's calculations and measurement for the  $1 \rightarrow 0$  transition in the (110) plane of 42.5-micron-thick diamond. The PCR calculations with dechanneling effects included are close to Azadegan's calculations and experimental data, but increase at a higher rate with beam energy.

1 $\rightarrow$ 0 Photon Yield (photons/e sr  $\times 10^{-3}$ )

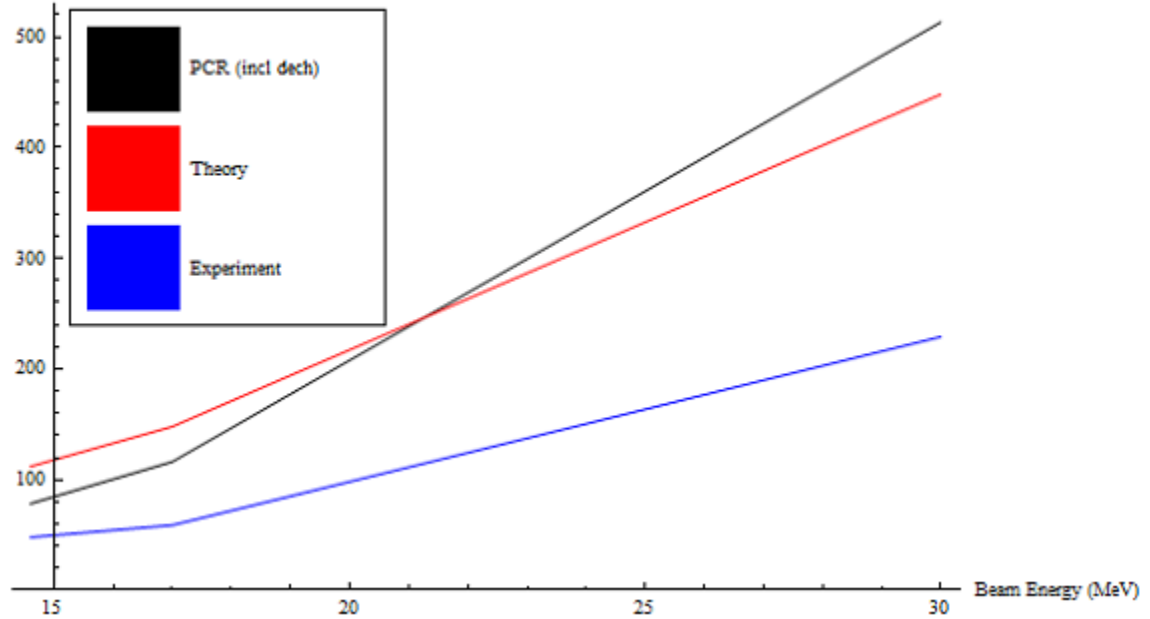


Figure 14: Photon yield comparison of PCR code, including dechanneling effects, with Azadegan's calculations and measurement for the  $1 \rightarrow 0$  transition in the (110) plane of 168-micron-thick diamond. The PCR calculations with dechanneling effects included are close to Azadegan's calculations and experimental data, but increase at a higher rate with beam energy.

1 $\rightarrow$ 0 Photon Yield (photons/e sr  $\times 10^{-3}$ )

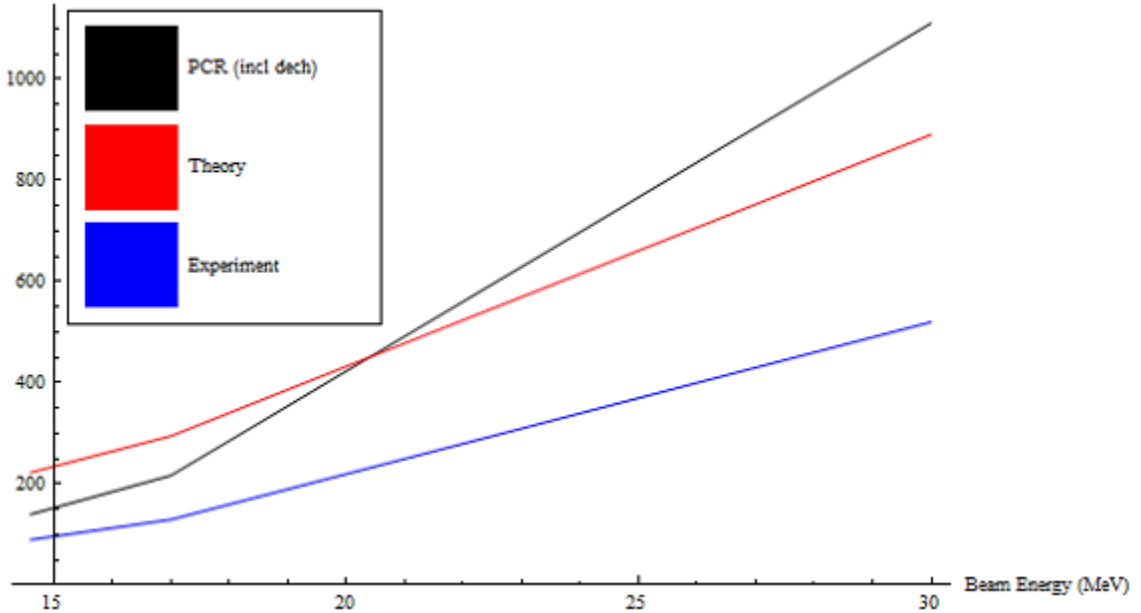


Table 6: PCR-calculated, including electron dechanneling; theoretically-calculated; and measured CR photon yields of the  $1 \rightarrow 0$  transition in the (110) plane of diamond.

$L$ ( $\mu\text{m}$ )	$Y_{PCR(incl\ dech)}$ (photons/e sr $\cdot 10^{-3}$ )	$Y_{calc}$ (photons/e sr $\cdot 10^{-3}$ )	$Y_{exp}$ (photons/e sr $\cdot 10^{-3}$ )
14.6 MeV			
42.5	78	112	48
168	140	223	90
17 MeV			
42.5	116	148	59
168	217	295	130
30 MeV			
42.5	513	448	229
168	1110	890	520

### 4.3 Including beam divergence

The PCR code assumes that the incoming electron beam has zero divergence; that is, the electrons have the same angle of incidence with the plane. This is unrealistic. The incidence angles of the electrons can be represented by a Gaussian function

$$f(\theta_0, \sigma, \theta) = \frac{1}{\sigma\sqrt{2\pi}} \exp\left(-\frac{(\theta - \theta_0)^2}{2\sigma^2}\right) \quad (34)$$

where  $\theta_0$  is the mean (expected) incidence angle and  $\sigma$  is the beam divergence.

The PCR code calculates the initial population,  $P_{i,0}(\theta)$ , of each quantum state  $i$  as a function of the incidence angle. To include a realistic beam divergence, the state populations can be averaged over the Gaussian function such as

$$P_{i,0}(\theta_0, \sigma) = \frac{\int f(\theta_0, \sigma, \theta) P_{i,0}(\theta) d\theta}{\int f(\theta_0, \sigma, \theta) d\theta} = \int f(\theta_0, \sigma, \theta) P_{i,0}(\theta) d\theta \quad (35)$$

where the integral can be taken over  $\theta_0 \pm 5\sigma$ . Initially, Mathematica had difficulty performing the integral in Eq. 35, but the authors have since resolved the issue.

## 5 Discussion

The progress made in improving the accuracy of the linewidth and photon yield calculations of the PCR code is promising, but not yet complete. In order to calculate accurate linewidths for planes other than (110) and crystals other than diamond, a more general expression for the rms multiple scattering angle for channeling must either be found or derived. The next step for the authors will be to create a fit expression for the ratio  $\theta_{ms,ch}/\theta_{ms}$  using Azadegan's data from Tab. 4. Then, calculating  $\theta_{ms}$  for different crystals will allow us to make a crude estimate of  $\theta_{ms,ch}$  for those crystals. This should not be seen as the final step in the calculation of  $\theta_{ms,ch}$  for different planes and crystals, and a more rigorous formulation should be sought.

Completing the photon yield updates will be more involved. Most importantly, the effect of electron dechanneling must be implemented. It is already known that the PCR code miscalculates the nonradiative transition rates (Eq. 26), because the selection rule is not consistent with the theory presented in Chouffani's paper. Namely, there should be nearly no non-radiative transitions between states with opposite parity, but a number of such transitions are seen in the PCR code. After the transition rates are fixed, an analysis of the accuracy of the first attempt (replacing Eq.

25 with Eq. 33) must be done. Secondly, a decision on whether or not to include the effect of photon self-absorption must be made. If it is decided that the effect is significant, then the issues of implementing it in the code for small crystal thicknesses must be solved. Finally, in order to calculate line shapes for crystals and planes other than the (110) plane of diamond, we must find a more general expression for  $\theta_{ms,ch}$ , as mentioned above.

After the line width and photon yield calculations are finalized, other beam and detector effects can be included. The divergence and energy spread of the beam were not included in the PCR code and would have significant effects on the CR simulation. The beam divergence effects the initial populations of quantum states and has been successfully implemented in the code, as described in Sec. 4.3. The energy spread of the beam is a source of line broadening that should be simple to include. The resolution of the detector is also a significant source of line broadening that will be simple to implement.

## 6 Conclusion

The goal of this project was to create a code for the simulation of channeling radiation in single crystals. The project consisted of three stages: 1) diagnosing the discrepancies between Azadegan's PCR code and the calculations that he cites in his dissertation, 2) understanding the sources of the discrepancies, and 3) producing solutions to the issues that are found and including beam and detector effects to make the simulations more realistic.

In diagnosing the discrepancies between the PCR code and Azadegan's calculations, it was found that the peak photon energies were consistent, but the PCR-calculated line widths were significantly smaller than the line widths cited in Azadegan's dissertation, and the PCR-calculated photon yields were significantly larger than those calculated in his dissertation.

The source of error in the line width calculations was found quickly. In the PCR code, Azadegan only included the line-broadening effects of coherence length, ignoring the effects of Bloch-wave broadening, multiple scattering, and other beam and detector effects that he describes in his dissertation. The sources of error in the photon yield calculations were not as easily discerned. It was quickly determined that Azadegan did not include the effect of photon self-absorption and used a Lorentzian line shape instead of the appropriate Lorentzian-Gaussian convolution. After closer inspection, it was also found that Azadegan did not include the effect of electron dechanneling due to multiple scattering.

To fix the line width calculations, Bloch-wave broadening and multiple scattering effects were included. For more realistic simulation, the detector resolution and energy spread of the beam will be included as well. To fix the photon yields, photon self-absorption was included, the Lorentzian line shape was replaced with a Lorentzian-Gaussian convolution, and the effect of electron dechanneling is in the process of being included in the state population dynamics. Finally, beam divergence was added.

There remain obstacles to fixing some of the problems. A general expression for the rms multiple scattering angle for channeling must be found in order to make accurate line width and line shape calculations. A satisfactory understanding of the dechanneling effect must also be found in order to fix the photon yields. Including the self-absorption of photons, the code will not run for small crystal thicknesses. The simplest of the obstacles will be to add the effects of detector resolution and energy spread of the beam.

Once these issues have been addressed, combining the improvements should be trivial and the project will be complete. Combining improved line width and photon yield calculations with realistic beam and detector effects should greatly improve the accuracy of the simulation code. An accurate and easily-accessible package for the simulation of CR spectra will facilitate the under-

standing of upcoming experiments at the A0 and ASTA facilities at Fermilab.

## 7 References

[1] Azadegan, Behnam. Investigation of Planar Channeling Radiation on Diamond and Quartz Crystals at Electron Energies between 14 and 34 MeV and Probing the Influence of Ultrasonic Waves on Channeling Radiation. Thesis. Print. Technical University, Dresden.

[2] Azadegan, Behnam. "A Mathematica Package for Calculation of Planar Channeling Radiation Spectra of Relativistic Electrons Channeled in a Diamond-structure Single Crystal (quantum approach)." **Computer Physics Communications** (2012): 1064-069.

[3] Azadegan, Behnam. PCR. Computer software. 29 Nov. 2012.

[4] Hubbell, J. H., and S. M. Seltzer. "Tables of X-Ray Mass Attenuation Coefficients and Mass Energy-Absorption Coefficients from 1 KeV to 20 MeV for Elements  $Z = 1$  to 92 and 48 Additional Substances of Dosimetric Interest." **Physical Measurement Laboratory** (1996).

[5] Chouffani, K., and H. Uberall. "Theory of Low Energy Channeling Radiation: Application to a Germanium Crystal." **Phys Stat. Sol.** **14** (1999): 107-51.

## 8 Acknowledgements

I would like to thank Dr. Tanaji Sen for his invaluable and continuing guidance in this project. I would also like to thank Dr. Eric Prebys, Carol Angarola, and everyone else who makes the Lee Teng program possible.